IEEE Access
Multidisciplinary | Rapid Review | Open Access Journal

Received April 21, 2021, accepted May 2, 2021, date of publication May 5, 2021, date of current version May 14, 2021.

Digital Object Identifier 10.1109/ACCESS.2021.3077644

Real-Time Artifact Removal System for Surface EMG Processing During Ten-Fold Frequency Electrical Stimulation

HAI-PENG WANG[1,2], ZHENG-YANG BI[3], WEN-JIE FAN[2], YI-XIN ZHOU[2], YU-XUAN ZHOU[3,4], FEI LI[2], KEPING WANG[2], (Senior Member, IEEE), XIAO-YING LÜ[3,5], AND ZHI-GONG WANG[2,5], (Senior Member, IEEE)

[1]School of Electronic and Information Engineering, Sanjiang University, Nanjing 210012, China
[2]Institute of RF- & OE-ICs, Southeast University, Nanjing 210096, China
[3]State Key Laboratory of Bioelectronics, Southeast University, Nanjing 210096, China
[4]Department of Biomedical Engineering, School of Biomedical Engineering and Informatics, Nanjing Medical University, Nanjing 211166, China
[5]Co-innovation Center of Neuroregeneration, Nantong University, Nantong 226001, China

Corresponding author: Zhi-Gong Wang (zgwang@seu.edu.cn) and Xiao-Ying Lü (luxy@seu.edu.cn)

This work was supported in part by the National Natural Science Foundation of China under Grant 61801262, Grant 81701806, Grant 61534003, and Grant 61874024; in part by the Natural Science Foundation of the Jiangsu Higher Education Institutions of China under Grant 18KJB510039; and in part by the Science and Technology Pillar Program of Jiangsu Province under Grant BE2016738.

ABSTRACT In this paper, three easily implemented hardware algorithms, including the adaptive prediction error filter based on the Gram-Schmidt algorithm (GS-APEF), the least mean square adaptive filter and the comb filter, are extensively investigated for artifact denoising on a constructed semi-simulated database with varied ten-fold frequency stimulation. By implementing the GS-APEF in the field-programmable gate array (FPGA) and using the edge noise mitigating technique, a stimulation artifact denoising system is designed to realize real-time stimulation artifact removal under varied ten-fold frequency functional electrical stimulation. Good performance of the artifact denoising is demonstrated in proof-of-concept experiments on able-bodied subjects with a mean correlation coefficient between the root mean square profile of denoised surface electromyography and volitional force of 0.94, verifying the validity of the proposed prototype.

INDEX TERMS Functional electrical stimulation (FES), stimulus artifact removal (SAR), surface electromyography (sEMG), adaptive filter, field-programmable gate array (FPGA).

I. INTRODUCTION

Closed-loop neuromodulation improves open-loop therapeutic electrical stimulation by delivering and adjusting stimulation parameters in response to a patient's neural state [1]. Since Liberson invented the first noninvasive functional electrical stimulation (FES) system for the heel drop correction of hemiplegic patients [2], FES has been used as a neuro-rehabilitation method for motor function in paralyzed patients following stroke and spinal cord injury (SCI) [3], and there is evidence that closed-loop FES with voluntary recipient involvement is vital for the success of therapy [4], [5]. Therefore, electromyography (EMG) has been used for designing proportional or autogenic EMG-controlled FES systems [6]–[9]. Recording volitional EMG (vEMG) from the stimulated muscle can provide non-invasive, more natural, and more physiologically appropriate continuous control of paretic muscles.

The stimulation response typically consists of a short, high-amplitude spike (direct artifact) followed by a slow, exponential decay (indirect artifact or residual artifact). The artifact mitigation methods for the neural signal modulation system have been reviewed by *Zhou et al.* [10]. In surface EMG (sEMG) controlled FES, the stimulation generates larger voltage electrical pulses (in the range of 0∼90 V) than common neural stimulation. As a result, the direct artifact may be many orders of magnitude larger than the underlying EMG. Therefore, the main challenge in vEMG recording during FES is that high voltage stimulation pulses generate immense amplitude interference accompanied with broadband spectrum distribution mixing with EMG [11]–[13]. In addition, the large amplitude stimulation pulses cause the recording amplifier to saturate rapidly and cannot be fully recovered during the interval [14]. The residual artifact is

The associate editor coordinating the review of this manuscript and approving it for publication was Norbert Herencsar.

also called the muscle response wave (M-wave), which is the composite of action potential signals owing to the simultaneous activation of many motor units (MUs) during electrically elicited contractions [14].

Some scientists have proposed various advanced algorithms to mitigate the stimulus artifact in surface EMG applications. These methods can be classified into four categories: (1) Blanking approaches: also called the blank window method, these methods are realized by disconnecting the input of the detecting circuit when electrical stimulation is performed or fulfilled by software way [14]. It is easy to implement the real time removal of simulation artifacts and prevent amplifier saturation. However, the EMG signal cannot be detected during the blanking time, and the long-term artifact can be only cancelled by extending the blanking time. This results in the reduction of the stimulation frequency (usually less than 20 Hz), loss of EMG signal and discontinuity of stimulation, and leads to strength limitation and discontinuity in the stimulated muscle [15]. In addition, the stimulation spike and M-wave are not likely to be completely separated. If the stimulation frequency is increased, the tail of the previous M-wave will be superimposed on the beginning of the next one, resulting in transients and distortion of the recorded signal [16]. (2) Subtractive approaches: the artifact templates are subtracted from the waveform to reveal the underlying signal. These methods were first introduced as offline techniques [17]–[19], and have been implemented in real-time software [20] and hardware [21]. In addition, the templates are mainly generated from the average artifacts [17]–[21]. (3) Filtering approaches: Fixed comb filters have been applied to remove M-waves under the assumption of stationary artifacts [22], [23]. Sennels [14] first proposed an adaptive filter based on least mean square (LMS) combined with blanking circuit for stimulus artifact removal (SAR) under a fixed-frequency stimulation. Qiu *et al.* designed an adaptive-matched filter via genetic algorithm (GA-AMF) [24], which can effectively extract EMG from the stimulated muscle and adjacent muscles. (4) Decomposition approaches: These techniques use high computational complexity algorithms, such as independent component analysis [25], wavelet [26], and empirical mode decomposition (EMD) [13], to decompose the mixed signal into uncorrelated elements. After the recognition and discarding of artifact-dominated components, the EMG signal can be reconstructed.

Recently, *Li et al.* proposed a stimulation artifact suppression algorithm combining the blanking and template subtraction approaches [12]. Spike detection and the first-order derivative analysis algorithm can adaptively calculate the blanking window length, and an autoregressive model is adopted to predict the subtracting template of the artifact under different stimulation intensities. Subsequently, *Zhou et al.* proposed an algorithm integrating the complete ensemble EMD with a logistic regression to realize vEMG extraction during the FES with time variant amplitudes and frequencies [27]. This is because in addition to the stimulation intensity, the frequency modulation can also play an important role in the stimulation strategy for force control and fatigue resistance [28], [29]. However, this decomposition-based technique requires high computational costs and time-consuming processing and is not suitable for real-time denoising applications. The main challenge in the closed-loop EMG controlled FES system design is the adaptive vEMG recording algorithm under the specific need for stimulations with time-variant parameters and implementation in the hardware with perfect real-time performance. The only real-time and effective removal of M-waves in the surface EMG extraction during FES is the adaptive prediction error filter based on the Gram-Schmidt algorithm (GS-APEF) with the use of blanking circuits [9], [30], [31]. However, this approach only has been verified under fixed frequency stimulation after it is implemented in a field-programmable gate array (FPGA) due to the corresponding filter coefficient. Therefore, stimulation of 20 Hz was taken as an example in the above references. In fact, the stimulation frequency range commonly used in clinical research is 20 $\sim$ 50 Hz, and the artifact removal performance using the GS-APEF algorithm with varied frequency stimulation has not been studied. In addition, considering the blanking technique limits the increase in stimulation frequency, research without the blanking method will be undertaken first.

In this paper, we mainly focus from the perspective of real-time artifact removal under varied frequency stimulation using an easily implemented hardware algorithm. For the workflow in our work, first, a detailed explanation of the GS algorithm showing denoising performance for the ten-fold frequency stimulation is presented. Then, three easily implemented algorithms (GS-APEF, LMS, and Comb filter) comparing artifact denoising performances on the constructed semi-simulated database with varied ten-fold frequency stimulation are investigated. Based on the FPGA implementation of the GS-APEF and the edge noise mitigating module, a stimulation artifact denoising system is proposed to realize real-time stimulus artifact removal under ten-fold varied frequency stimulation. Its performance using real experimental FES application on able-bodied subjects is tested.

II. METHODS

A. SUBJECTS

Six healthy subjects (five males, one female, 27.67$\pm$2.94 years, 72.17$\pm$7.86 kg) participated in the study. The subjects were asked to refrain from any strenuous exercise of the upper extremities for at least 24 hours before the study. They provided written informed consent before participation, and this study was approved by the ethical committee of Southeast University.

B. DATA COLLECTION SETUP

The subject was seated upright with their right hand placed at the experimental desk. The stimulation pulses were generated by the isolated constant current stimulator (model 4100,

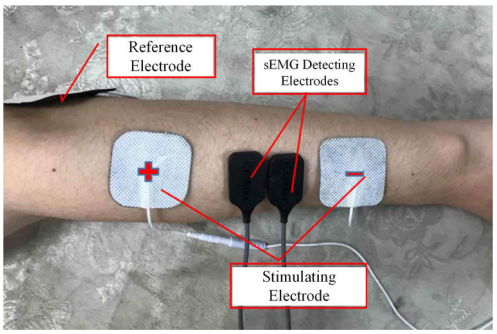

FIGURE 1. Photograph of the attachment configuration of the detection and stimulation electrodes for collecting EMG data.

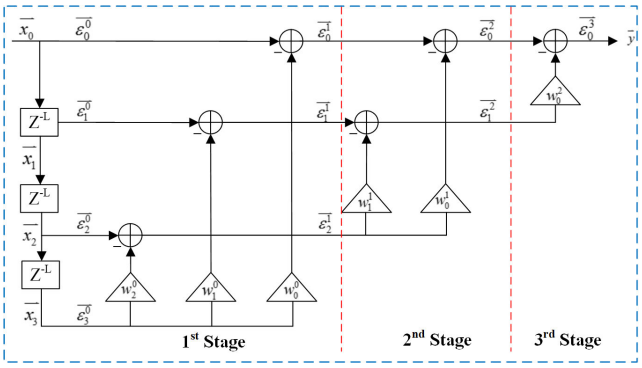

FIGURE 2. The signal flow of the 3rd-order GS algorithm (adapted from[30]).

A-M Systems, WA). The EMG recording system (Bagnoli^{TM}, Delsys Inc., Natick, MA) with band-pass filtering from 20 to 500 Hz and amplification with a gain of 1000 was used to detect the EMG. As illustrated in Fig. 1, one bipolar surface Ag/AgCl electrode was placed on the detection sites, and the gelled stimulation electrodes (4×4 cm^2) of one channel were fixed on the extensor carpal ulnar (ECU) of the right upper extremity with the distance of 5 cm. EMG signal data were converted using a 12-bit analog-to-digital NI USB-6009 data acquisition board (National Instruments Corp., Austin, Texas) at a sample rate of 1 kHz and recorded by a custom-designed LabView 2011 subprogram.

C. ANALYSIS OF GS-APEF DENOISING ARTIFACTS UNDER DIFFERENTIAL FREQUENCY STIMULATION

The principle of the M-order GS-APEF filter has been described in detail by Yeom et al [30], [31]. The input signal of N-length is equally divided into $(M+1)$ segments, where each segment includes $L = N/(M+1)$ indicating the length of data. Fig. 2 illustrates the signal flow of 3rd-order GS algorithm. The input data is divided into (3+1) segments, and can be denoted by an L-length vector $\{(\overrightarrow{x_i}, 0 \le i \le M\}$. The filter weight w_i^m is obtained by orthogonal calculation of the GS algorithm. The output of each stage is the product of the estimated vector minus the reference vector and the weight. Each iteration output will reduce an L-length vector, and finally give the vector of unit length. The iterative calculation formula of the GS algorithm can be expressed as follows [30], [31]:

$$\overrightarrow{\varepsilon_i^0} = \overrightarrow{x_i}, \quad i = 0, 1, \ldots, M \tag{1}$$

$$w_i^m = \frac{\overrightarrow{\varepsilon_i^{mT}} \cdot \overrightarrow{\varepsilon_{M-m}^m}}{\left\| \overrightarrow{\varepsilon_{M-m}^m} \right\|^2}, \quad m = 0, 1, \ldots, M-1; i = 0, 1, \ldots M-m-1 \tag{2}$$

$$\overrightarrow{\varepsilon_i^{m+1}} = \overrightarrow{\varepsilon_i^m} - w_i^m \cdot \overrightarrow{\varepsilon_{M-m}^m}, \quad m = 0, 1, \ldots, M-1; i = 0, 1, \ldots M-m-1 \tag{3}$$

The superscript m represents the m^{th}-level operation in Fig. 2, and the subscript i represents the specific order in each level of operation. Finally, the output of the GS-APEF filter is $\overrightarrow{y} = \overrightarrow{\varepsilon_0^m}$, and it is the extracted EMG signal.

In the practical realization, L can be set as the ratio of the data sampling frequency f_{sample} to the stimulation frequency f_{stim}. The rationale for choosing L can be deduced as the number of samples between consecutive stimulation pulses. However, once the GS-APEF filter is implemented in the FPGA, the parameter L and order M should be constant,and these fixed parameters ($L = 50, M = 1, 3, 6$) were tested only for the simulation frequency of 20 Hz [30], [31]. Considering the design should be simultaneously adapted to the varied frequency stimulation and facilitate hardware implementation, L should be set as an integer for the filter. Here, the value of 50 is selected as the data segment length ($L = 50$ ms) under the sampling rate f_{sample} of 1 kHz. In addition, the latency between the controller and controlee is within 350 ms, which is adequate for real-time neural prostheses control [32]. Thus the maximum filter order M is 6 according to the following equation:

$$L \times (M+1) \le 350\text{ms} \tag{4}$$

We derive that the denoising performance of GS-APEF with stimulation frequency f_{stim} should meet the following conditions:

$$L \times P = \frac{f_{sample}}{f_{stim}} Q, \quad 1 \le P \le M \tag{5}$$

where P and Q are integers, which means that the window length of P processing segments must equal the length of the Q cycle stimulus response, so that the filter can adaptively find the right template for artifact removal. Otherwise, the mitigation performance is very poor. Additionally, the realized filter order M' for f_{stim} is M/P, instead of M.

According to Eq. (5), the detailed principle of GS-APEF denoising artifacts with different stimulation frequencies is illustrated in Fig. 3. For the 6$^{\text{th}}$-order filter ($M = 6$) and the stimulation frequencies of 20 Hz, 40 Hz, 30 Hz, 50 Hz, 25 Hz, 35 Hz, and 45 Hz, the realized filter orders are $M' = 6, 6, 3, 3, 1, 1$ and 1, respectively. For the 3$^{\text{rd}}$-order filter ($M = 3$), the M's values are 3, 3, 1 and 1 for $f_{\text{stim}} = 20$ Hz, 40 Hz, 30 Hz and 50 Hz, respectively. Therefore, the 6$^{\text{th}}$-order

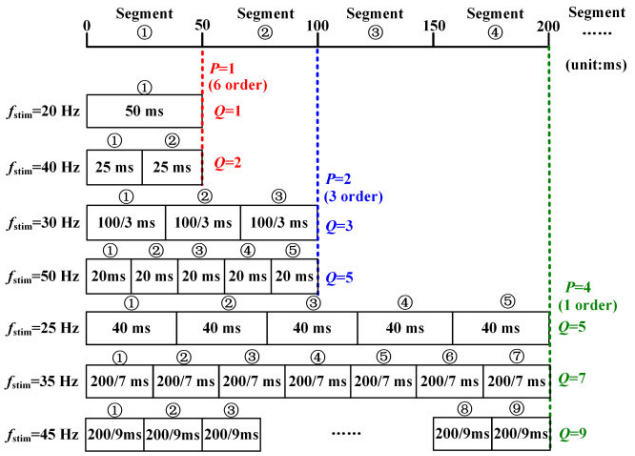

FIGURE 3. Principle of GS-APEF denoising artifact under different stimulation frequencies ($L = 50$, $f_{\text{sample}} = 1$ kHz).

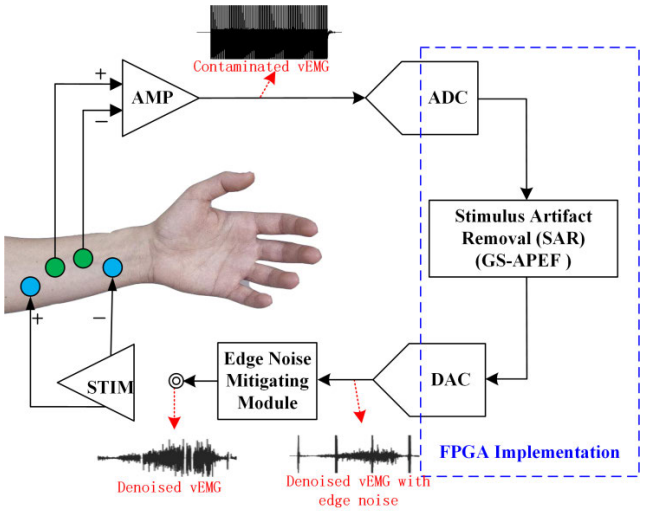

FIGURE 4. Diagram of the open-loop real-time artifact removal prototype for surface EMG processing during ipsilateral functional electrical stimulation.

GS algorithm shows better artifact mitigation capability than the 3rd-order algorithm for these frequencies. Additionally, the filter cannot remove the artifact noise for the stimulation frequencies of 25Hz, 35 Hz, and 45 Hz at an order M of 3 because the value of P exceeds M. In addition, the algorithm cannot be applied to FES with other random frequencies, such as 23 Hz, 34 Hz and 47 Hz, because it cannot satisfy Eq. (5) even for the 6th-order filter.

D. PROTOTYPE AND FPGA IMPLEMENTATION

1) PROTOTYPE OVERVIEW

Fig. 4 illustrates the block diagram of the open-loop real-time stimulus artifact removal (SAR) prototype for surface EMG processing. The instruments for sEMG detection and FES stimulation are mentioned in Section 2B. The contaminated EMG signal is converted to digital data by an analog-to-digital converter (ADC). Through stimulus artifact removal using the FPGA implementation of the GS-APEF algorithm, the filtered EMG signal with edge noise is then generated by a digital-to-analog converter (DAC) under the control of FPGA. According to the analysis mentioned above, the 6th-order GS-APEF with $f_{\text{sample}} = 1$ kHz and $L = 50$ is implemented in an AL515 FPGA board (ALINX Inc., Shanghai, China), which contains an Altera Cyclone IV EP4CE5F17C8L FPGA. A high-speed AN108 AD/DA board (ALINX Inc., Shanghai, China) containing an AD9280 and an AD9708 (Analog Devices, Inc., Norwood, MA) is used for the digital data acquisition and analog signal generation in the prototype. In addition, an edge noise mitigating module implemented in a micro-controller unit (MCU) board is connected with the output of the DAC. It can effectively suppress the output edge noise at the stimulation start/end and stimulation frequency alternation. When the denoised vEMG data are obtained, the time-domain features of denoised vEMG can modulate the varied frequency stimulation. Therefore, this prototype makes it possible to realize an adaptive closed-loop

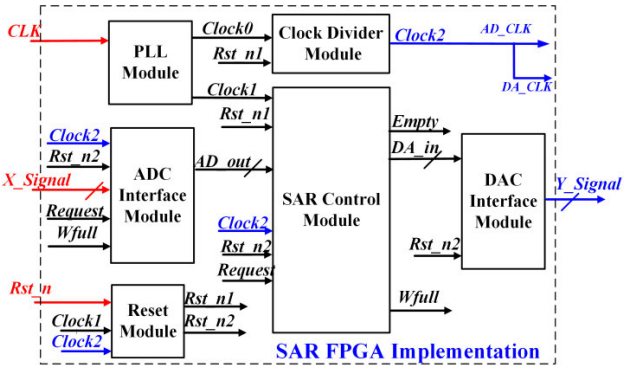

FIGURE 5. Representative block diagram of stimulus artifact removal (SAR) is implemented in FPGA.

EMG-controlled FES system for the continuous control of ipsilateral paretic muscles.

2) FPGA IMPLEMENTATION

The representative architecture of the proposed real-time SAR module is shown in Fig. 5. It adopts the top-down design approach and mainly consists of a phase-locked loop (PLL) module, a clock divider module, a reset module, a SAR control module, an ADC interface module, and a DAC interface module. The input signals include contaminated EMG signal (*X_Signal*), external reset signal (*Rst_n*) and external clock (*CLK*, 50 MHz). The main output signal is voluntary sEMG signal (*Y_Signal*) with artifact rejection. The FPGA has a high-performance clock management unit and rich clock tree routing resources. In order to reduce clock skew and ensure smooth layout, the PLL module is used to generate a clock signal (*Clock1*, 150 MHz) and *Clock2* is set to 3 kHz for the ADC and DAC interfaces.

The SAR control module performs artifact mitigation to obtain the digital vEMG signal, which means the whole GS

algorithm is implemented in this submodule. The schematic of the 1st-order GS-APEF implementation on FPGA is presented by Yeom [30, 31], and it includes two multiplications. However, according to Fig. 2 and Eq. (1)-(3), the 6th-order GS-APEF algorithm actually performs 21 elementary processing units (42 multiplications in total) within multiple iterations on 7 equal-length vectors. In addition, the GS-APEF has a large number of vectors processed at one time, and the amount of data in the intermediate operation results is also large. For the FPGA where multiplier resources are inherently limited, this method is challenging for simultaneous processing of multiple channels. Therefore, there are architectural tradeoffs between high mitigation performance, low resource utilization, low start-up latency, and multi-channel processing.

Here, the architecture with core processing unit reuse method is presented to solve this trade-off. The suitable iterative structure, asynchronous first-in-first-output (FIFO), built-in multiport random access memory (RAM), and finite state machine optimization are all incorporated in the SAR module design. There is only one elementary processing unit implemented in the FPGA for one-channel processing. The core processing unit will perform multiple iterations on the seven equal-length vectors to obtain 50 discrete vEMG data sets. Then, the calculation result is stored in the post-stage asynchronous FIFO under the slow driving clock (*Clock2*). Finally, the DAC interface module is used to convert the digital signal into an analog signal.

3) EDGE NOISE MITIGATION

Finally, in order to suppress the output edge noise at the stimulation start/end and stimulation frequency alternation, a post-processing of output filtered vEMG data using threshold comparison method is added to generate the final denoised vEMG data. When the filtered vEMG data output from GS-APEF exceeds the threshold, the final denoised data in a subsequent short time window will be kept at zero to mitigate the interference of the output edge noise caused by the GS-APEF algorithm.

E. SIMULATION AND EXPERIMENTAL TEST PROCEDURE

1) GS-APEF DENOISING ARTIFACT WITH DIFFERENT STIMULATION FREQUENCIES

In order to validate the denoising artifact performance of the GS-APEF algorithm based on our analysis described in Section IIC, a test with different stimulation frequencies is carried out, and the pure stimulation response data are recorded under the condition of the subject staying fully relaxed during stimulation, without variations resulting from volitional force exertion. The stimulation frequency f_{stim} is selected as 20 Hz, 40 Hz, 30 Hz, 50 Hz, 25 Hz, 35 Hz, and 45 Hz. Three random frequencies including 23 Hz, 34 Hz and 47 Hz, are also investigated in the test. In addition, given that an unbalanced pattern can lead to a transient artifact with a lasting exponential decay [10], monopolar negative stimulation pulses with constant 400 μs pulse width are adopted, and the amplitude is 10 mA with 100 continuous stimulation pulses. The duration of one stimulation frequency test is about 6 s.

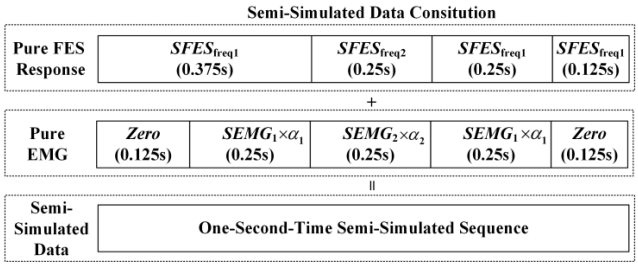

FIGURE 6. The constitution of one-second-time semi-simulated data.

2) SIMULATION TEST OF DENOISING ARTIFACT WITH VARIED STIMULATION FREQUENCIES

The semi-simulated data are constructed to access the GS-APEF algorithm and compared with other two filters, including comb filter [22], [23] and LMS adaptive filter (LMS-AF) [14]. These two filters are classical algorithms and can be implemented in hardware for real-time SAR. The parameters of GS and LMS are all set with $L = 50$ and $M = 6$, and the comb filter is selected as 20Hz for the comparison. The semi-simulated data are built upon two databases: the stimulation response database and pure EMG database. The pure stimulation response data are recorded similarly with the method mentioned above, except that the stimulation frequency f_{stim} varies from 20 Hz to 50 Hz with a step size of 10 Hz, and the amplitude varies from 7 mA to 10 mA with a step size of 1 mA. For the pure vEMG database, the subject is instructed to perform three maximal voluntary contractions (MVC) in wrist flexion, and the vEMG of 30% MVC is sampled.

One-second-time semi-simulated data are set up according to the protocol [27] as illustrated in Fig. 6. The two pure FES responses with different stimulation frequencies ($SFES_{\text{freq1}}$ and $SFES_{\text{freq2}}$) are selected from the stimulation response database, and two weighted vEMG data ($SEMG_1$ and $SEMG_2$) are chosen from the pure EMG database. The two weights α_1 and α_2 can be calculated as follows:

$$\alpha_1 = \frac{SD(SFES_{\text{freq1}})}{SD(SEMG_1) \times r} \tag{6}$$

$$\alpha_2 = \frac{SD(SFES_{\text{freq2}})}{SD(SEMG_2) \times r} \tag{7}$$

where r is a varied constant and the two weights can be referred to as the standard deviation of FES response data and the standard deviation of the vEMG data ratio.

In addition, the two pure FES responses constructed in the semi-simulated data are under the same conditions of stimulation amplitude. This means that in the throughout the stimulation process, the amplitude stays constant with varied frequency stimulation. Therefore, for each FES to vEMG

ratio r (4, 8, 12, 16 and 20), ten semi-simulated sequences are setup by randomly selecting the FES response under stimulation by different pulse amplitudes and frequencies and in combination with pure EMG data. Finally, a total of fifty testing trains are constructed.

3) EXPERIMENTAL TEST OF REAL FES APPLICATION ON ABLE-BODIED SUBJECTS

The real-time SAR test was performed on six able-bodied subjects to validate denoising performance. Fig. 7 shows the experimental setup with the proposed FPGA prototype based on the 6th-order GS algorithm. The instruments are mentioned in ''Section IIB''. The subjects were told to perform a three times voluntary wrist extension task under voice prompts. Simultaneously, monopolar pulse stimulation sequences with constant amplitude and varied frequency were delivered to ECU during voluntary force exertion. The frequency was increased by 10 Hz every 2 s from 20 Hz to 50 Hz over 8 s, and then decreased to 20 Hz in the next 8s. The amplitude and pulse width of the monopolar stimulation were set as 7 mA and 400 μs due to the guarantee of eliciting wrist extension less than 30% MVC for all subjects. The test was repeated two times for each subject. In addition, the parameters of the edge noise mitigation module are set according to the measured DAC output, which is controlled by the FPGA running the GS-APEF algorithm. The threshold is set as 1V, and the length of the blanking time window is 120 ms. Furthermore, EMG signals contaminated by stimulation pulses were recorded through another bipolar surface Ag/AgCl electrode (Fig. 1), which was placed near the detection sites for comparison and analysis. Simultaneously, the wrist-joint force represented by the isometric wrist torque was acquired by a custom-made device in our lab [28] and can be used to calculate the cross-correlation coefficient between the volitional force and the denoised EMG signal.

F. PERFORMANCE EVALUATION

1) EVALUATION ON SIMULATION TEST

The denoising performance of the GS-APEF algorithm on semi-simulated data is compared with the performances of the comb filter and LMS adaptive filter. Two metrics are used to quantify the performance of these methods [27]: Signal to noise ratio (*SNR*) is defined as the ratio of average energy of pure vEMG $e(t)$ to that of noise, and the pre and post *SNR* of SAR are calculated as:

$$SNR_{\text{pre}}(\text{dB}) = 10\log_{10}\frac{\sum e(t)^2}{\sum (x(t)-e(t))^2} \tag{8}$$

$$SNR_{\text{post}}(\text{dB}) = 10\log_{10}\frac{\sum e(t)^2}{\sum (y(t)-e(t))^2} \tag{9}$$

where $x(t)$ is the one-second-time semi-simulated data, and $y(t)$ is the denoised signal data. Analogously, the normalized root mean square error (*NRMSE*) is also defined to investigate the average difference between the pure vEMG and the output filtered EMG.

$$NRMSE_{pre} = \frac{\sqrt{\sum (x(t)-e(t))^2/N}}{SD(e(t))} \tag{10}$$

$$NRMSE_{post} = \frac{\sqrt{\sum (y(t)-e(t))^2/N}}{SD(e(t))} \tag{11}$$

where N is the total length of data, and $SD(e(t))$ means the standard deviation of the pure vEMG data.

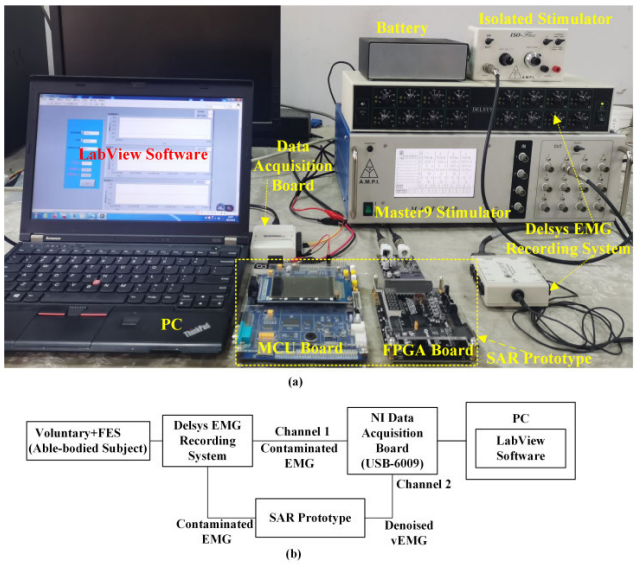

FIGURE 7. Real-time on-line SAR experiment configuration using the proposed prototype based on GS-APEF. (a) Photograph of the real-time experiment configuration. (b) Testing process of real-time experiment.

2) EVALUATION OF THE EXPERIMENTAL TEST FOR REAL FES APPLICATION

For the denoising trail using the proposed real-time SAR prototype, the contaminated sEMG, filtered EMG and wrist-joint force data are all recorded. Then, in order to mitigate the output edge noise at the stimulation start/end and the changes in stimulation frequency, post-processing of output filtered EMG data using threshold comparison method is added to generate the final denoised EMG data. The proposed system is evaluated by comparing the root mean square (RMS) profile of the final denoised EMG data and the force data using the Pearson correlation coefficient [13]. In addition, the continuous wavelet transform (wavename = 'cmor3-3') is used to investigate the time frequency representation of the contaminated sEMG signal and the final denoised EMG signal.

G. STATISTICAL ANALYSIS

To investigate the denoising performance of simulation test, a two-way analysis of variance (ANOVA) is implemented on two metrics results (*SNR* and *NRMSE*). The two factors are three SAR methods and five FES to vEMG ratio r. For the trial in able-bodied subjects, the difference between the EMG and force correlation coefficient and repetitions is analyzed

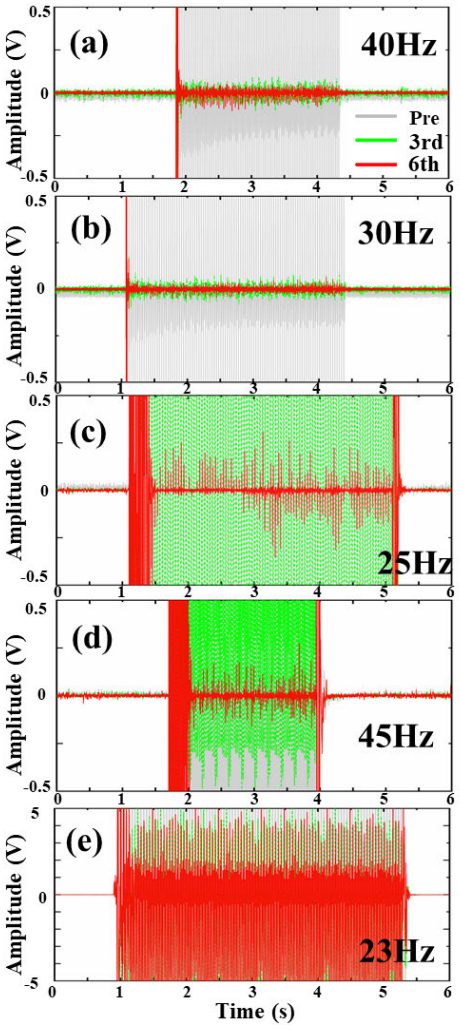

FIGURE 8. The illustration of the denoising performance of the GS-APEF algorithm (3rd-order and 6th-order) on pure stimulation response data with different frequencies. (a)-(e) Typical stimulation frequency of 40 Hz, 30 Hz, 25 Hz, 45 Hz, and 23 Hz.

using one-way ANOVA. The statistical analysis is performed with SPSS statistics 25 software (IBM corp., Chicago, IL, USA). The results are reported as the mean ± SD. Differences with $P \leq 0.05$ are considered significant.

III. RESULTS

A. PERFORMANCE EVALUATION OF TEST WITH DIFFERENT STIMULATION FREQUENCIES

According to the realized filter order M' depicted in Fig. 3, the denoising performance of the GS-APEF algorithm on pure stimulation response data with five typical stimulation frequencies are selected and illustrated in Fig. 8(a)-(e), including 40Hz ($M' = 6$), 30 Hz ($M' = 3$), 25 Hz, 45 Hz ($M' = 1$), and 23 Hz. For each typical frequency, the original stimulation response (gray), and the processed results of the 3rd-order (green) and 6th-order (red) of the GS-APEF ($L = 50$) are shown in each subfigure.

Because the original data contain only the stimulation response without volitional force exertion, the ideal noise-removal data is the baseline signal. We observe that the GS algorithm has good denoising performances for 40 Hz and 30Hz except the intrinsic edge noise at the beginning, and in particular, the curves processed by the 6th-order algorithm are closer to the baseline. For the 25 Hz and 45 Hz, the 3rd-order GS algorithm (green line) does not work in Fig. 8(c) and (d), and the mitigation capability using the 6th-order filter is worse, while the processed data are far greater than the baseline, due to the real filter order of 1. Finally, the processed data for $f_{\text{stim}} = 23$ Hz have the same amplitude with the original signal, which proves that the GS-APEF is not applicable for random frequency stimulation. Hence the test results are consistent with Fig. 3 as mentioned in Section IIC. Therefore, four ten-fold frequencies (20 Hz, 30 Hz, 40 Hz and 50 Hz) are adopted in the varied frequency stimulation test.

B. PERFORMANCE EVALUATION ON SIMULATION TEST WITH VARIED FREQUENCY STIMULATION

Fig. 9 shows an example selected from the constituted one-second-time semi-simulated database. The pure stimulation response data is recorded under the amplitude of 8 mA and monopolar negative stimulation pulses with constant 400μs pulse width. The two stimulation frequencies are 40 Hz and 30 Hz (Fig. 9a). As illustrated in Fig. 9(c), the semi-simulated sequence data consist of the stimulation response data plus the pure EMG data (Fig. 9b) with the FES to vEMG ratio of 4. It can be clearly observed that the volitional EMG signal is completely submerged in the stimulation artifact response.

Fig. 10 illustrates the filtered signals using three means on the semi-simulated data (described in Fig. 9) and pure vEMG under the ration r of 4. In Fig. 10(a), the time-domain waveforms of vEMG signal (red) extracted by GS-APEF are more similar to the original pure vEMG (green) than the LMS-AF and comb filter. However, the edge noise can be clearly observed at the transition of alternating stimulation frequency by using the GS-APEF and LMS-AF (e.g. around 0.375 s and 0.625 s). The edge noise generated by the LMS filter is much larger than the GS algorithm. The frequency domain of the semi-simulated data, pure vEMG, and denoised signals are obtained through Fourier transformation (Fig. 10b). Among the three methods, the spectrum of the denoised signal (red) also demonstrated a closer similarity to that of pure EMG (green). In addition, according to Fig. 10b, the fundamental frequency component of 40 Hz and the harmonic frequency components have higher power in the spectrum of the pre semi-simulated data (gray area), while those of 30 Hz and the harmonic components are much smaller. This is due to the stimulation frequency of 40 Hz occupying the most time in the stimulation sequence. Similar to the time domain, it can be observed that the frequencies of 30 Hz and harmonic components are still high in the denoised signal, which is caused by the generated edge noise.

Fig. 11 presents the SNR and NRMSE before and after processing with three mitigation methods under different FES

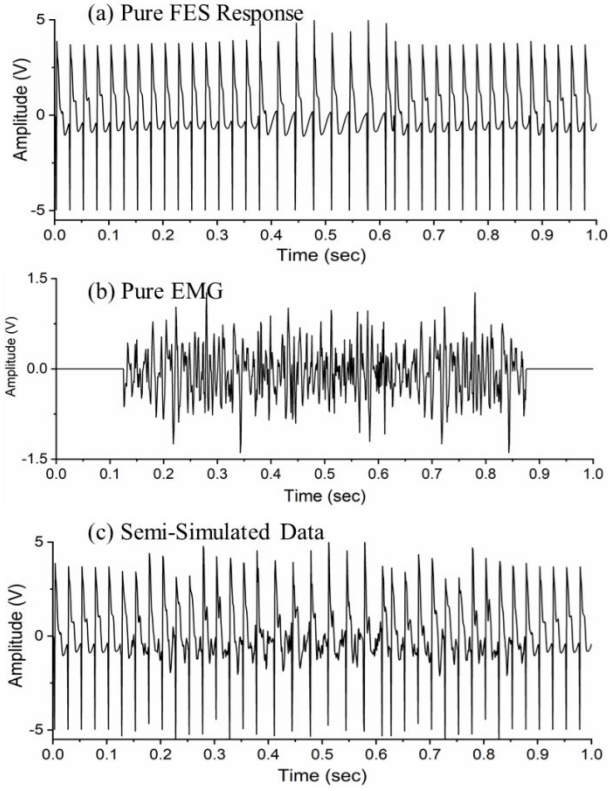

FIGURE 9. An example selected from the constituted one-second-time semi-simulated database. (a) The pure stimulation response data with constant amplitude of 8 mA and changing frequencies ($SFES_{freq1} = 40$ Hz, $SFES_{freq2} = 30$ Hz). The waveforms are monopolar negative stimulation pulses with constant 400 μs pulse width. (b) The pure EMG data. (c) The semi-simulated sequence setup with the combination of pure stimulation response data and pure EMG data with the FES to vEMG ratio ($r = 4$).

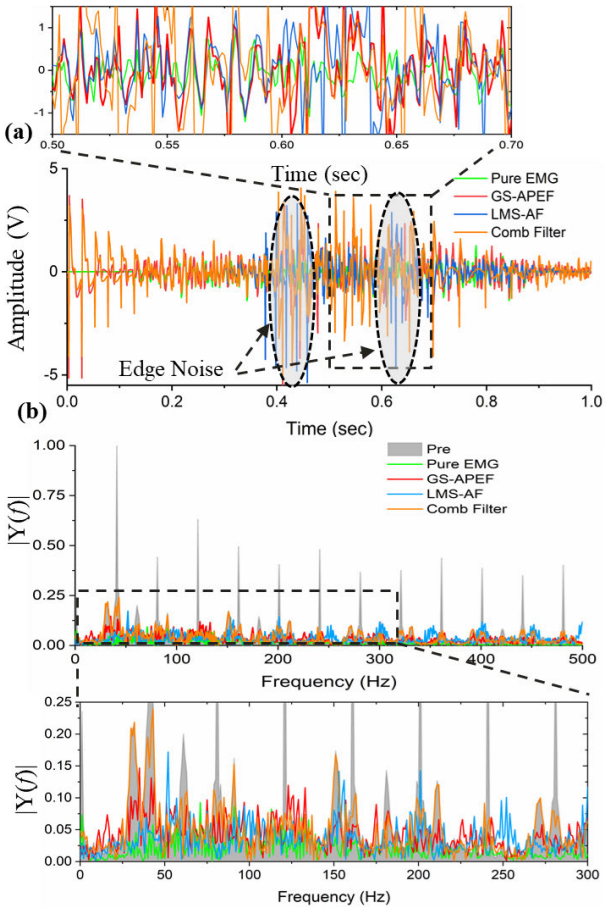

FIGURE 10. The illustration of the denoising performance of the GS-APEF algorithm on semi-simulated data (depicted in Fig. 7) compared with LMS adaptive filter and comb filter. (a) The time waveforms of the vEMG signal extracted by three methods and the pure EMG data. (b) The frequency domain of the above signals under Fourier transformation.

to EMG ratios. By using the GS-APEF, the *SNR* of filtered EMG ranged from -15.26 ± 3.87 dB to -46.19 ± 6.53 dB (n = 10), and the *NRMSE* ranged from 2.28 ± 0.36 to 11.35 ± 2.22 (n = 10). From Fig. 9, the GS-APEF and LMS-AF have nearly same denoising performance based on the two metrics.

A two-way ANOVA test is carried out to observe the influence of the FES to vEMG ratio (5 levels: 4, 8, 12, 16, 20) and the SAR method (3 levels: GS-APEF, LMS-AF, Comb filter) on *SNR* and *NRMSE*. There is a statistically significant interaction between the FES to vEMG ratio and denoising method on *SNR* (SAR method: $F(2,135) = 49.148$, $p < 0.001$; FES to vEMG ratio: $F(4,135) = 191.722$, $p < 0.001$) and *NRMSE*(SAR method: $F(2,135) = 54.90$, $p < 0.001$; FES to vEMG ratio: $F(4,135) = 162.954$, $p < 0.001$). However, there is no SNR and NRMSE evidence of significant interactions between the denoising method (GS-APEF and LMS-AF) and the FES to vEMG ratio ($p > 0.05$). Simple mean effects analysis shows no significant difference in *SNR* and *NRMSE* between the GS-APEF and LMS-AF ($p > 0.05$). Therefore, the evaluation test indicates that the GS-APEF and LMS-AF methods have similar denoising performance. In addition, both the *SNR* and *NRMSE* are significantly influenced by the FES to vEMG ratio r when using the two methods.

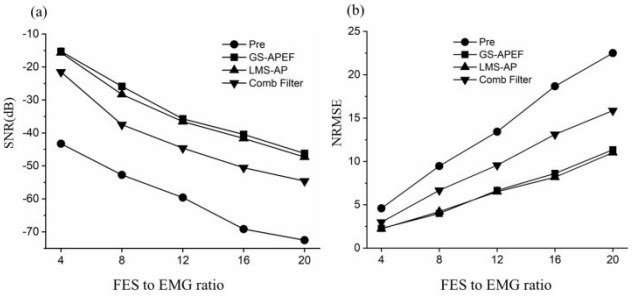

FIGURE 11. Statistical SAR performance evaluation of GS-APEF, LMS-AF, and comb filter on the simulation test. (a) Signal to noise ratio (*SNR*) and (b) normalized root mean square error (*NRMSE*) between pure vEMG and filtered EMG with different FES to vEMG ratios ($r = 4, 8, 12, 16, 20$).

C. PERFORMANCE EVALUATION BY AN EXPERIMENTAL TEST OF REAL FES APPLICATION

The surface EMG signals from six healthy subjects during the varied frequency stimulations are extracted in real-time using

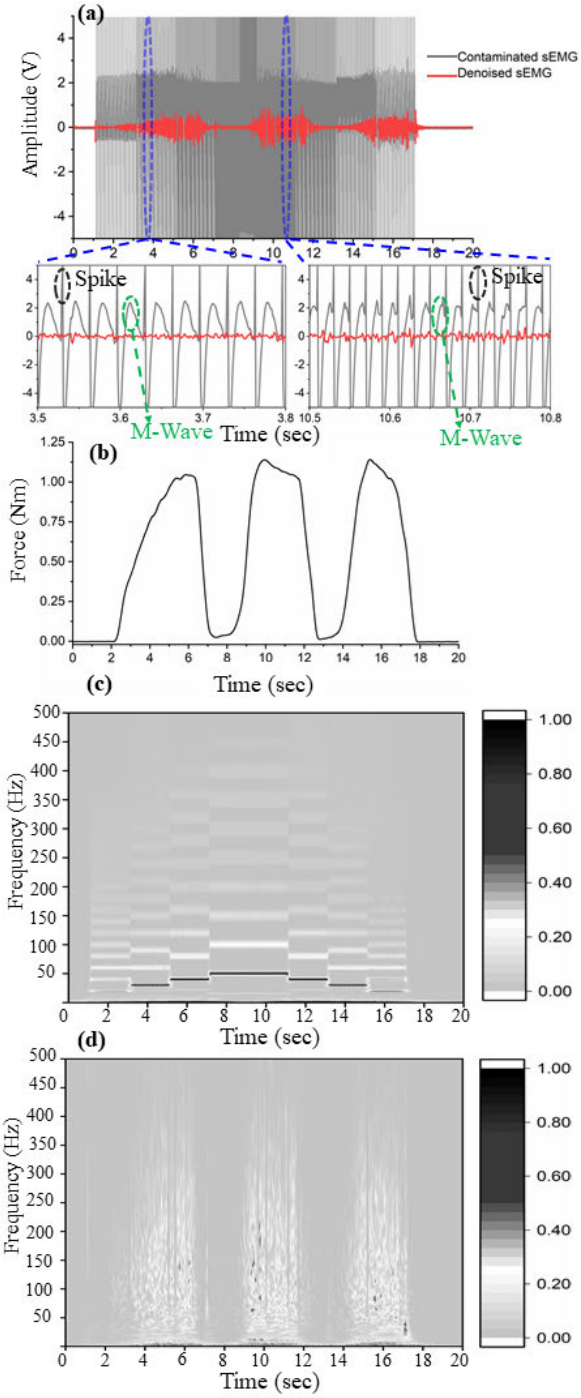

FIGURE 12. The representative denoising experimental results of real FES application on one able-bodied subject using the proposed SAR prototype. (a) The waveforms of pre contaminated sEMG signal and the corresponding denoised signal. (b) The corresponding recorded torque of wrist extension during the experimental test. (c) The corresponding time-frequency plot of pre contaminated sEMG signal. (d) The corresponding time-frequency plot of denoised sEMG signal.

the proposed SAR prototype. The waveforms of pre contaminated sEMG signal and the corresponding denoised sEMG signal in one able-bodied subject are illustrated in Fig. 12(a).

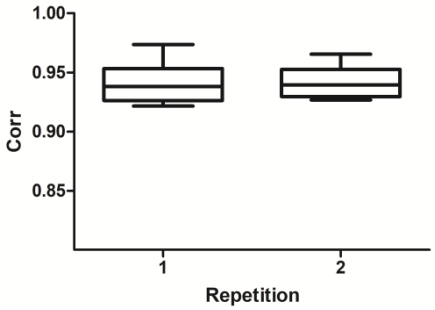

FIGURE 13. The cross-correlations between the RMS profiles of final denoised sEMG and the wrist extension torque in six able-bodied subjects with two repetitions.

The stimulation starts at 1 s and end at 17 s, and the stimulation frequency increases from 20 Hz to 50 Hz and decreases from 50 Hz to 20 Hz with a step size of 10 Hz. Each frequency is maintained for 2 s. It is obvious that the proposed SAR prototype can extract the volitional sEMG during three voluntary wrist extensions from the input signal contaminated with stimulation artifacts. Compared with the filtered signal (Fig. 10a), the output edge noise at the stimulation start/end and stimulation frequency alternation are also effectively removed by using the edge noise mitigation module. The time-frequency diagrams of contaminated and denoised sEMG signal are presented in Fig. 12(c) and (d), respectively. The high energy color components of stimulation frequency can be observed with the variations in time before denoising in Fig. 12(c). From Fig. 12(d), by using the SAR system with GS-APEF, the phenomenon of high-energy color in the EMG frequency band (20-450 Hz) is highly correlated with the wrist extension torque shown in Fig. 12(b).

The cross-correlations between the RMS profile of final denoised sEMG and the wrist extension torque are computed and analyzed in Fig. 13. The correlation coefficients between the denoised sEMG and force in the two repetitions are 0.94 ± 0.02 and 0.94 ± 0.01, respectively. According to the one-way ANOVA test, no significant difference is found between the EMG and force correlation coefficient. Therefore, it can be verified that the proposed real-time stimulation artifact denoising system can effectively and efficiently suppress the artifact noise for sEMG processing during ten-fold FES.

IV. DISCUSSION

In this study, a real-time stimulus artifact removal prototype under the varied ten-fold frequency FES is presented by implementing the GS-APEF algorithm in the FPGA and using the edge noise mitigating method. The GS-APEF is chosen because it uses less hardware and fewer numerical operations than other adaptive algorithms, and it has been implemented in the FPGA platform [30], [31]. In particular, compared with previous studies, the artifact removal capability is extended from a stimulation frequency of 20 Hz not only to ten-fold frequency but also can achieve varied ten-fold frequency stimulation without using the blanking method,

based on extensive investigation of the GS algorithm and experimental tests.

A previous study by *Yeom et al.* observed that the parameter L in the GS-APEF can be adjusted as the ratio of the data sampling frequency to different stimulation frequencies [30], [31]. However, it is challenging to implement the algorithm in the FPGA for artifact denoising with different stimulation frequencies due to the varied filter coefficients. In addition, the blanking method was also used in previous studies and the blanking time reduced and limited the increase of stimulation frequency. Therefore, previous studies only used GS-APEF at the stimulation frequency of 20 Hz. In contrast to these studies, we obtain an intriguing finding and derive Eq. (5) to explain the relationship between denoising performance of GS-APEF and stimulation frequency under the fixed parameter L, as illustrated in Fig. 3. The results shown in Fig. 8 indicate that the 6^{th}-order GS algorithm has good denoising performance for the ten-fold frequency with the realized orders of 6 and 3. For the frequencies of 25Hz, 35 Hz, and 45 Hz, the algorithm actually only demonstrates an effect of the 1^{st}-order filter. In addition, it is not applicable to other random frequency stimulations. Therefore, from the perspective of denoising performance of the algorithm, we emphasize the ''ten-fold'' frequency stimulation.

In order to illustrate whether the algorithm can effectively remove the influence of M-waves, Fig. 12a is partially enlarged and inserted as two insets in the results. The input contaminated sEMG signal contains the full stimulation response, including the direct artifact (stimulation spike) and the residual artifact (M-wave). In the two insets, the short 5V spike is caused by large amplitude stimulation pulses and detected by a recording amplifier. The M-wave is also the composite of action potential signals owing to the simultaneous activation of many MUs during electrically elicited contractions. Therefore, the magnitude of the M-wave should be of the same order as the voluntary EMG signal. In our work, the slow exponential decay signal followed by the spike should be the M-wave. The magnitude of the M-wave is slightly larger, mainly because of the rapid saturation of the recording amplifier and necessary recovery process in the absence of the blanking technique. Therefore, the GS-APEF can effectively remove the influence of M-waves, even in cases in which the blanking method is not used.

As shown in Fig. 10 and Fig. 11, the statistical and evaluation tests indicate GS-APEF and LMS-AF have comparable artifact denoising performance under varied stimulation frequencies. However, the LMS adaptive filter algorithm requires accurately estimating the autocorrelation matrix and solving the inverse of the matrix [14]. Therefore, the disadvantage of LMS-AF is the need to perform a large number of complex data calculations such as matrix QR/LU decomposition and forward and backward replacement [14], which would prohibit real-time and multi-channel application. The GS-APEF has the potential for real-time artifact cancellation while using far less hardware or, similarly, requiring fewer numerical operations than the LMS adaptive algorithm [9].

In addition, the output edge noise is an inherent problem of the adaptive filter, including the GS-APEF and LMS-AF. It is mainly caused by the mismatch in the filter template at the stimulation start/end and stimulation frequency alternation. Therefore, in order to solve this issue, an edge noise mitigating module is adopted. It uses the threshold comparison method to trigger a short-time blanking window and can easily run on an MCU platform. According to our experiment, the normal amplitude of the output denoising signal is below 0.8V. Therefore, the threshold is set as 1V, and the short-time blanking window is 120 ms, considering the tradeoff between the signal integrity and denoising. This method can effectively mitigate the interference of the output edge noise caused by the adaptive algorithms.

Nevertheless, the present study had some limitations. First, regarding the influence of FES on EMG properties, most traditional EMG-controlled FES systems use the envelope of the sEMG signal to modulate the stimulation parameters, including amplitude, pulse-width or frequency [7], [8]. Therefore, as long as the denoised EMG is highly correlated with force signal, FES is considered to have little influence on EMG properties in this controlled strategy. For the other controlled FES methods based on EMG time or frequency domains, e.g., the frequency and intensity co-modulation strategy [28], [29], it is necessary to further investigate whether this method can provide consistent muscle force control in the case of artifact denoising in the closed-loop EMG-controlled FES system. Second, only the ten-fold frequency stimulation is used in our work. In a future study, we will research how to remove the FES artifact covering the whole frequency band (20 $\sim$ 60 Hz) in real time. Third, the design is only for one-channel stimulation application, and the feasibility of extending to two-channel FES or more is not investigated. Furthermore, the influence of cross-talk between channels on the algorithm will be studied in the future.

V. CONCLUSION

In this paper, three algorithms (GS-APEF, LMS-AF and Comb filter), which are easy to implement in hardware, are extensively investigated for artifact denoising under varied frequency stimulation. By implementing the adaptive prediction error filter based on the Gram-Schmidt algorithm in the FPGA and the edge noise mitigating technique, a real-time stimulation artifact denoising system is designed. The mean correlation coefficient between the denoised sEMG and volitional force is 0.94. It is expected that the proposed system has latent abilities in the adaptive closed-loop EMG-controlled FES system for the continuous control of ipsilateral paretic muscles using different stimulation frequencies and waveforms.

REFERENCES

[1] A. Zhou, S. R. Santacruz, B. C. Johnson, G. Alexandrov, A. Moin, F. L. Burghardt, J. M. Rabaey, J. M. Carmena, and R. Muller, ''A wireless and artefact-free 128-channel neuromodulation device for closed-loop stimulation and recording in non-human primates,'' *Nature Biomed. Eng.*, vol. 3, no. 1, pp. 15–26, 2019.

[2] W. Liberson, "Functional electrotherapy: Stimulation of the peroneal nerve synchronized with the swing phase of the gait of hemiplegic patients," *Arch. Phys. Med.*, vol. 42, pp. 101–105, Feb. 1961.
[3] O. Schuhfried, R. Crevenna, V. Fialka-Moser, and T. Paternostro-Sluga, "Non-invasive neuromuscular electrical stimulation in patients with central nervous system lesions: An educational review," *J. Rehabil. Med.*, vol. 44, no. 2, pp. 99–105, 2012.
[4] J. S. Knutson, M. Y. Harley, T. Z. Hisel, S. D. Hogan, M. M. Maloney, and J. Chae, "Contralaterally controlled functional electrical stimulation for upper extremity hemiplegia: An early-phase randomized clinical trial in subacute stroke patients," *Neurorehabilitation Neural Repair*, vol. 26, no. 3, pp. 239–246, Mar. 2012.
[5] S. C. McGie, J. Zariffa, M. R. Popovic, and M. K. Nagai, "Short-term neuroplastic effects of brain-controlled and muscle-controlled electrical stimulation," *Neuromodulation, Technol. Neural Interface*, vol. 18, no. 3, pp. 233–240, Apr. 2015.
[6] S. Saxena, S. Nikolic, and D. Popovic, "An EMG-controlled grasping system for tetraplegics," *J. Rehabil. Res. Develop.*, vol. 32, p. 17, Feb. 1995.
[7] R. Thorsen, R. Spadone, and M. Ferrarin, "A pilot study of myoelectrically controlled FES of upper extremity," *IEEE Trans. Neural Syst. Rehabil. Eng.*, vol. 9, no. 2, pp. 161–168, Jun. 2001.
[8] Y. Hara, S. Obayashi, K. Tsujiuchi, and Y. Muraoka, "The effects of electromyography-controlled functional electrical stimulation on upper extremity function and cortical perfusion in stroke patients," *Clin. Neurophysiol.*, vol. 124, no. 10, pp. 2008–2015, Oct. 2013.
[9] H. Yeom and Y.-H. Chang, "Autogenic EMG-controlled functional electrical stimulation for ankle dorsiflexion control," *J. Neurosci. Methods*, vol. 193, no. 1, pp. 118–125, Oct. 2010.
[10] A. Zhou, B. C. Johnson, and R. Muller, "Toward true closed-loop neuromodulation: Artifact-free recording during stimulation," *Current Opinion Neurobiol.*, vol. 50, pp. 119–127, Jun. 2018.
[11] A. Shadmani, V. Viswam, Y. Chen, R. Bounik, J. Dragas, M. Radivojevic, S. Geissler, S. Sitnikov, J. Muller, and A. Hierlemann, "Stimulation and artifact-suppression techniques for *in vitro* high-density microelectrode array systems," *IEEE Trans. Biomed. Eng.*, vol. 66, no. 9, pp. 2481–2490, Sep. 2019.
[12] Y. Li, J. Chen, and Y. Yang, "A method for suppressing electrical stimulation artifacts from electromyography," *Int. J. Neural Syst.*, vol. 29, no. 06, Aug. 2019, Art. no. 1850054.
[13] R. Pilkar, M. Yarossi, A. Ramanujam, V. Rajagopalan, M. B. Bayram, M. Mitchell, S. Canton, and G. Forrest, "Application of empirical mode decomposition combined with notch filtering for interpretation of surface electromyograms during functional electrical stimulation," *IEEE Trans. Neural Syst. Rehabil. Eng.*, vol. 25, no. 8, pp. 1268–1277, Aug. 2017.
[14] S. Sennels, F. Biering-Sorensen, O. T. Andersen, and S. D. Hansen, "Functional neuromuscular stimulation controlled by surface electromyographic signals produced by volitional activation of the same muscle: Adaptive removal of the muscle response from the recorded EMG-signal," *IEEE Trans. Rehabil. Eng.*, vol. 5, no. 2, pp. 195–206, Jun. 1997.
[15] Y. Muraoka, "Development of an EMG recording device from stimulation electrodes for functional electrical stimulation," *Frontiers Med. Biol. Eng.*, vol. 11, no. 4, pp. 323–333, 2001.
[16] F. Mandrile, D. Farina, M. Pozzo, and R. Merletti, "Stimulation artifact in surface EMG signal: Effect of the stimulation waveform, detection system, and current amplitude using hybrid stimulation technique," *IEEE Trans. Neural Syst. Rehabil. Eng.*, vol. 11, no. 4, pp. 407–415, Dec. 2003.
[17] E. B. Montgomery, J. T. Gale, and H. Huang, "Methods for isolating extracellular action potentials and removing stimulus artifacts from microelectrode recordings of neurons requiring minimal operator intervention," *J. Neurosci. Methods*, vol. 144, no. 1, pp. 107–125, May 2005.
[18] Y. Erez, H. Tischler, A. Moran, and I. Bar-Gad, "Generalized framework for stimulus artifact removal," *J. Neurosci. Methods*, vol. 191, no. 1, pp. 45–59, Aug. 2010.
[19] T. Hashimoto, C. M. Elder, and J. L. Vitek, "A template subtraction method for stimulus artifact removal in high-frequency deep brain stimulation," *J. Neurosci. Methods*, vol. 113, no. 2, pp. 181–186, Jan. 2002.
[20] S. Culaclii, B. Kim, Y.-K. Lo, and W. Liu, "A hybrid hardware and software approach for cancelling stimulus artifacts during same-electrode neural stimulation and recording," in *Proc. 38th Annu. Int. Conf. IEEE Eng. Med. Biol. Soc. (EMBC)*, Aug. 2016, pp. 6190–6193.
[21] K. Limnuson, H. Lu, H. J. Chiel, and P. Mohseni, "Real-time stimulus artifact rejection via template subtraction," *IEEE Trans. Biomed. Circuits Syst.*, vol. 8, no. 3, pp. 391–400, Jun. 2014.
[22] P. E. Crago, R. J. Nakai, and H. J. Chizeck, "Feedback regulation of hand grasp opening and contact force during stimulation of paralyzed muscle," *IEEE Trans. Biomed. Eng.*, vol. 38, no. 1, pp. 17–28, Jan. 1991.
[23] W. Peasgood, T. Whitlock, A. Bateman, M. E. Fry, R. S. Jones, and A. Davis-Smith, "EMG-controlled closed loop electrical stimulation using a digital signal processor," *Electron. Lett.*, vol. 36, no. 22, pp. 1832–1833, Oct. 2000.
[24] S. Qiu, J. Feng, R. Xu, J. Xu, K. Wang, F. He, H. Qi, X. Zhao, P. Zhou, L. Zhang, and D. Ming, "A stimulus artifact removal technique for SEMG signal processing during functional electrical stimulation," *IEEE Trans. Biomed. Eng.*, vol. 62, no. 8, pp. 1959–1968, Aug. 2015.
[25] K. Zeng, D. Chen, G. Ouyang, L. Wang, X. Liu, and X. Li, "An EEMD-ICA approach to enhancing artifact rejection for noisy multivariate neural data," *IEEE Trans. Neural Syst. Rehabil. Eng.*, vol. 24, no. 6, pp. 630–638, Jun. 2016.
[26] M. Yochum and S. Binczak, "A wavelet based method for electrical stimulation artifacts removal in electromyogram," *Biomed. Signal Process. Control*, vol. 22, pp. 1–10, Sep. 2015.
[27] Y. Zhou, Z. Bi, M. Ji, S. Chen, W. Wang, K. Wang, B. Hu, X. Lu, and Z. Wang, "A data-driven volitional EMG extraction algorithm during functional electrical stimulation with time variant parameters," *IEEE Trans. Neural Syst. Rehabil. Eng.*, vol. 28, no. 5, pp. 1069–1080, May 2020.
[28] Y.-X. Zhou, H.-P. Wang, X.-L. Bao, X.-Y. Lü, and Z.-G. Wang, "A frequency and pulse-width co-modulation strategy for transcutaneous neuromuscular electrical stimulation based on sEMG time-domain features," *J. Neural Eng.*, vol. 13, no. 1, Feb. 2016, Art. no. 016004.
[29] L. A. Johnson and A. J. Fuglevand, "Mimicking muscle activity with electrical stimulation," *J. Neural Eng.*, vol. 8, no. 1, Feb. 2011, Art. no. 016009.
[30] H. J. Yeom, Y. C. Park, Y. R. Yoon, T. M. Shin, and H. R. Yoon, "An adaptive M-wave canceler for the EMG controlled functional electrical stimulator and its FPGA implementation," in *Proc. 26th Annu. Int. Conf. IEEE Eng. Med. Biol. Soc.*, Sep. 2004, pp. 4122–4125.
[31] H. Yeom, "Gram-Schmidt M-wave canceller for the EMG controlled FES," *IEICE Trans. Inf. Syst.*, vols. 88, no. 9, pp. 2213–2217, Sep. 2005.
[32] A. D. Koutsou, S. Summa, B. Nasser, J. G. Martinez, and M. Thangaramanujam, "Upper limb neuroprostheses: Recent advances and future directions," *Emerging Therapies in Neurorehabilitation, Biosystem & Biorobotics*, vol. 4. Berlin, Germany: Springer, 2014, pp. 207–233.

HAI-PENG WANG received the B.S. degree in electronic engineering from the Shandong University of Science and Technology, Qingdao, China, in 2009, the M.S. degree in electronic engineering from Xidian University, Xi'an, China, in 2012, and the Ph.D. degree in circuits and systems from the Institute of RF- & OE-ICs, Southeast University, Nanjing, China, in 2017. From 2017 to 2019, he worked as a Lecturer with the School of Electronic and Information Engineering, Sanjiang University, Nanjing. Since September 2019, he has been working as a Postdoctoral Fellow with the State Key Laboratory of Millimeter Waves, Southeast University. His research interests include electromagnetic metasurfaces, deep learning, biomedical circuits and systems design, and biomedical signal processing.

ZHENG-YANG BI received the B.S. degree in biomedical engineering from the Heifei University of Technology, Heifei, China, in 2013, and the M.S. degree in biomedical engineering from Southeast University, Nanjing, China, in 2016, where he is currently pursuing the Ph.D. degree with the School of Biomedical Engineering. His research interests include biomedical circuits and systems design and biomedical signal processing.

WEN-JIE FAN received the B.S. degree in electronic engineering from the South China University of Technology, Guangzhou, China, in 2015, and the M.S. degree in electronic engineering from Southeast University, Nanjing, China, in 2018. Since June 2018, he has been working with Marvell Automotive BU, Shanghai, China. He currently focus on automotive AISC design.

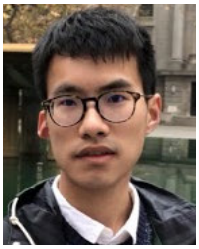

YI-XIN ZHOU received the B.S. degree in electronic information engineering from Tianjin Polytechnic University, Tianjin, China, in 2016. He is currently pursuing the Ph.D. degree with the Institute of RF- & OE-ICs, Southeast University, Nanjing, China. His research interests include charge pump and neural stimulator for bio-medical applications.

YU-XUAN ZHOU received the B.S. degree in mechanical engineering and automation from the Nanjing University of Science and Technology, Nanjing, China, in 2007, the M.S. degree in biomedical engineering from Nanjing Medical University, Nanjing, in 2010, and the Ph.D. degree in biomedical engineering from Southeast University, Nanjing, in 2016. He is currently a Lecturer in biomedical engineering with Nanjing Medical University. His research interests include the biomedical signal processing, neural rehabilitation systems, and flexible electronic devices.

FEI LI received the B.E. and M.E. degrees in circuits and systems from Southeast University, Nanjing, China, in 2002 and 2005, respectively, and the Ph.D. degree in physical electronics from Tokyo Institute of Technology, Tokyo, Japan, in 2013. In 2005, he joined the Institute of RF- & OE-ICs, Southeast University. His research interest is mixed signal circuits, medical electronics and circuits, intelligent CMOS sensors, and data readout circuits.

KEPING WANG (Senior Member, IEEE) received the B.S. degree in electronic engineering from Southeast University, Nanjing, China, in 2003, the M.S. degree in information science and electronic engineering from Zhejiang University, Hangzhou, China, in 2006, and the Ph.D. degree in information science and engineering from Southeast University, in 2010.

From 2010 to 2012, he has been working as a Research Fellow with Nanyang Technological University, Singapore, and as a Research Associate with Wireless Sensing Laborator, University of Washington, Seattle, USA, from 2012 to 2016. From January 2017 to September 2019, he was an Associate Professor with Southeast University of China, and has been promoted to a Full Professor with the Tianjin University of China, since September 2019. He has authored or coauthored over 50 international journals and conference papers, five patents, and one book chapter. His research interests include future wireless bio-electrical interfaces, body-area-networks, automotive and home monitoring, and implantable devices demand wireless technology well beyond the state-of-the-art. He was a member of Academic Council, School of Information Science and Engineering, Southeast University. He serves as an Associate Editor for IEEE Access.

XIAO-YING LÜ was born in Shanghai, China. She received the M.-Med. degree from Shanghai Second Medical University, in 1986, and the Dr.-Dent. degree from Freiburg University, Freiburg, Germany, in 1996. From 1996 to 1997, she made her postdoctoral researching work with Freiburg University. In 1997, she became an Associate Professor with Southeast University, China. Since 2003, she has been a Full Professor.

ZHI-GONG WANG (Senior Member, IEEE) was born in Henan, China. He received the M.Eng. degree in radio engineering from the Nanjing Institute of Technology (currently, Southeast University), Nanjing, China, in 1981, and the Dr.-Ing. degree in electronic engineering from Ruhr-University Bochum, Germany, in 1990.

From 1977 to 1981, he worked on radio communication techniques and computer aided circuit designs with Nanjing Institute of Technology. From 1985 to 1990, he worked on high-speed silicon bipolar circuit designs for multigigabit/s optic fiber communication with Ruhr-University Bochum. From October 1990 to September 1997, he was with the Fraunhofer Institute for Applied Solid State Physics, Freiburg, Germany, where he was involved with high-speed GaAs integrated circuits (ICs) for optic-fiber data transmission and monolithic microwave integrated circuits (MMICs). Since October 1997, he has been a Full Professor with Southeast University. He has been a Guest Professor for over 20 universities in China, Canada, and Australia. He has authored or coauthored over 20 books and over 400 SCI/EI/ISTP-indexed articles. He holds over 30 Chinese, European, US, and Japanese patents. He has recently been involved with IC design for optic-fiber transmission systems, for RF wireless, microwave, and millimeter-wave applications, and in microelectronic systems for biomedical applications. He is a member of Chinese Expert Committee of the Internet of Things for Healthy and the Chairman of the Advisory Committee of Electrical and Electronical Basic Courses of Chinese Universities.